



Treball Final de Grau

Synthesis and characterization of supramolecular assemblies of cobalt(II).

Síntesis i caracterització d'assemblatges supramoleculars de cobalt(II).

Núria Capó Serrano

June 2021



UNIVERSITAT DE
BARCELONA

B:KC Barcelona
Knowledge
Campus
Campus d'Excel·lència Internacional

Aquesta obra esta subjecta a la llicència de:
Reconeixement–NoComercial–SenseObraDerivada



<http://creativecommons.org/licenses/by-nc-nd/3.0/es/>

"I am among those who think that science has great beauty. A scientist in his laboratory is not only a technician, he is also a child place before natural phenomenon, which impress him like a fairy tale."

Marie Curie

Primer de tot vull agrair a la Leoni Barrios per donar-me l'oportunitat de poder participar en aquest projecte de recerca, del qual tant he après. Així com al grup de GMMF per acollir-me i aconsellar-me durant tot el procés. A més m'agradaria agrair als meus companys de laboratori Manto Maniaki i Joan Cardona pels ànims i suport.

També m'agradaria donar les gràcies a la meva família i als amics que he conegut durant la carrera i amb qui tants bons moments he compartit.

REPORT

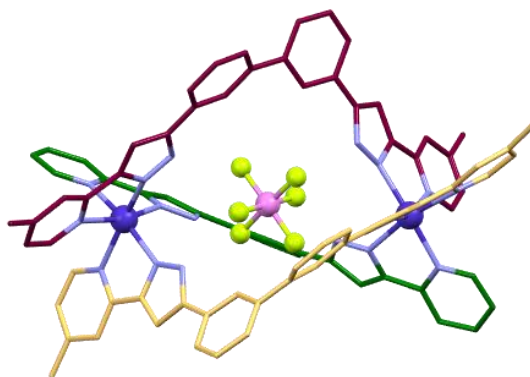
CONTENTS

1. SUMMARY	3
2. RESUM	5
3. INTRODUCTION	7
3.1. Slow Relaxation of Magnetization: SMM features	7
3.2. Spin Crossover	9
3.3. Host-Gest Systems: Looking for the multifunctionality	11
4. OBJECTIVES	12
5. EXPERIMENTAL SECTION.	12
5.1. Materials and methods	12
5.1.1. Infrared Spectroscopy	12
5.1.2. Mass Spectrometry	13
5.1.3. Single-Crystal X-ray diffraction	13
5.1.4. ¹⁹ F NMR Spectroscopy	13
5.1.6. Magnetic measurements	13
5.2. Synthesis of metallocomplexes	14
5.2.1. Synthesis of ClO ₄ @[Co ₂ (L2) ₃](ClO ₄)(OH) ₂ (CH ₃ O)·nCH ₃ OH (1)	14
5.2.2. Synthesis of ClO ₄ @[Co ₂ (L3) ₃](ClO ₄) ₂ (CH ₃ O)·nCH ₃ OH (2)	14
5.2.3. Synthesis of SiF ₆ @[Co ₂ (L1)(L3) ₂](PF ₆) ₂ (3)	15
5.2.3.1. Attempt of synthesizing PF ₆ @[Co ₂ (L1)(L3) ₂](PF ₆) ₃	15
5.2.3.2. Attempt of synthesizing BF ₄ @[Co ₂ (L1) ₂ (L3)](BF ₄) ₃	15
6. SYNTHESIS DISCUSSION	16
7. CRYSTAL STRUCTURES	18
7.1. Crystal structure of ClO ₄ @[Co ₂ (L2) ₃](ClO ₄)(OH)(CH ₃ O)·nCH ₃ OH (1)	18
7.2. Crystal structure of ClO ₄ @[Co ₂ (L3) ₃](ClO ₄) ₂ (CH ₃ O)·nCH ₃ OH (2).	20
7.3. Crystal structure of SiF ₆ @[Co ₂ (L1)(L3) ₂](PF ₆) ₂ ·nCH ₃ OH (3)	23
8. ¹⁹F NMR SPECTROSCOPY	25

9. MASS SPECTROMETRY	26
10. MAGNETIC PROPERTIES	26
10.1. Magnetic measurements for $\text{ClO}_4@[\text{Co}_2(\text{L}3)_3](\text{ClO}_4)_2(\text{CH}_3\text{O}) \cdot n\text{CH}_3\text{OH}$ (2)	27
10.2. Magnetic measurements for $\text{SiF}_6@[\text{Co}_2(\text{L}1)(\text{L}3)_2](\text{PF}_6)_2 \cdot n\text{CH}_3\text{OH}$ (3)	28
11. CONCLUSIONS	33
12. REFERENCES AND NOTES	34
13. ACRONYMS	37
APPENDICES	41
Appendix 1: IR spectra	41
Appendix 2 : MALDI spectra	43

1. SUMMARY

Supramolecular chemistry is based on weak interactions formed between molecules. In this area, a new series of Cobalt(II)-based helicates have been developed, which due to its intramolecular interactions and the properties of cobalt can lead to interesting magnetic properties, such as behaving as Single Molecular Magnets (SMMs) or presenting spin transition (SCO). This work describes the synthesis and characterization of three assemblies acting as host-guest systems including their magnetic study. To this end, the ligands L1, L2 and L3 ligands have been used to form Cobalt(II) dinuclear helicates, capable of holding different anions in their cavities. Although in one case the intention was the encapsulation of BF_4^- and PF_6^- , it has been found that heteroleptic helicates have a strong template effect towards the encapsulation of SiF_6^{2-} , over which the charge 2- may be a key component in their high stability. Therefore, this opens a new line of research to understand better how template effect works in heteroleptic systems.

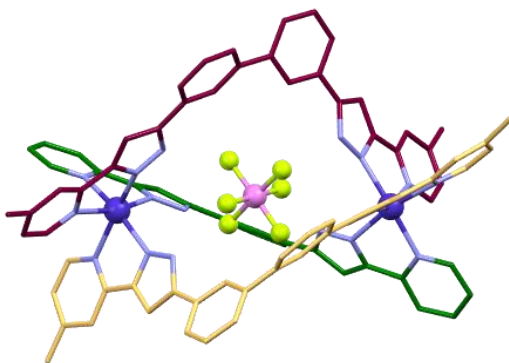


$\text{SiF}_6@[\text{Co}_2(\text{L1})(\text{L3})_2]^{2+}$ compound where L1 is shown in green color and L3 in yellow and purple, cobalt ions are shown in dark blue.

Keywords: Supramolecular chemistry, cobalt(II) dinuclear helicate complexes, host-guest systems, template effect, heteroleptic helicates.

2. RESUM

La química supramolecular està fonamentada en les interaccions febles formades entre molècules. En aquesta àrea, s'ha desenvolupat una nova sèrie d'helicats basats en cobalt(II), que a causa de les interaccions intramoleculares i a les propietats del cobalt poden donar lloc a propietats magnètiques, comportant-se com a imàns moleculars (Single Molecular Magnets, SMMs) o presentant transició d'espín (SCO). Aquest treball descriu la síntesi i caracterització de tres assemblatges actuant com a sistemes anfitrió-convidat (host-guest) inclouent el seu estudi magnètic. Per a això s'han utilitzat els lligands L1, L2 i L3 per formar helicats dinuclears de cobalt(II), capaços d'albergar en el seu interior diferents anions en la seva cavitat. Tot i que en un dels casos la intenció era l'encapsulament de BF_4^- i PF_6^- , s'ha trobat que els helicats heterolèptics presenten un fort efecte template cap a l'encapsulament de SiF_6^{2-} , sobre el qual la carrega 2- podria ser un component clau en la seva alta estabilitat. Això obre pas a una nova línia de recerca per tal de conèixer millor com aquest efecte template funciona en sistemes heterolèptics.



Compost $\text{SiF}_6@[\text{Co}_2(\text{L1})(\text{L3})_2]^{2+}$ on apareix L1 en verd i L3 en groc i lila i els ions cobalt estan marcats en blau fosc.

Paraules clau: Química supramolecular, helicats dinuclears de cobalt (II), sistemes host-guest, efecte template, helicats heterolèptics.

3. INTRODUCTION

Since the emergence of supramolecular chemistry, transition metal helicates have become a central topic not only for their potential applications, but also because of their great importance in understanding self-assembly processes and searching for new supramolecular devices.^{1,2} This field offers an attractive strategy to design molecular assemblies with especially relevant properties, such as spin crossover (SCO) and slow relaxation of the magnetization. Thus, single molecular devices are regarded to be the future of nanoscale spintronic.

In the recent years, the search for this kind of devices has also extended to cobalt compounds. Since this research field began, cobalt compounds have been obviated and very few have been synthesized.³ However, novel Co(II) compounds have demonstrated to be a good candidates for the development of these devices, not only for their promising magnetic properties but also because of its abundance and stability.⁴

3.1 SLOW RELAXATION OF THE MAGNETIZATION: SMM FEATURES

Since the first single-molecular magnet (SMM), the well-known Mn_{12} cluster was discovered,⁵ a large number of compounds displaying such behavior have been reported. The Grup de Magnetisme I Molècules Funcionals, GMMF group, has focused part of its efforts on developing multifunctional molecules presenting this phenomenon.⁶⁻⁹ The extensive interest on SMMs stems from their potential applications for ultrahigh-density devices, quantum computing and molecule spintronics.¹⁰

SMMs are based on paramagnetic metal complexes of the *d* and *f* block elements, with large energetic barriers (U_{eff}). When these species are exposed to a magnetic field, their spin changes: they become magnetized. Once the magnetic field is removed, the magnetization is retained for a certain time only below a specific temperature, which is called the blocking temperature.

Magnetic behavior of slow relaxations has to be understood as an energetic wall, which needs to be overcome in order to reach the equilibrium of spin states M_S . Such wall is determined by the total spin of the molecule (*S*) and the magnetic anisotropy (*D*), thus, the larger the energetic effective barrier is (U_{eff}), the slower the relaxation will occur. For this reason, the interest in this field has focused on searching complexes with a high magnetization barrier and practically no contribution from quantum tunneling to magnetization relaxation. The presence of a barrier is evidenced by the hysteresis loop when the field is swept in reverse. But more commonly, the

SMM behavior can be followed by measurements of frequency using ac magnetic field, as will be carried out in the present work.

The relaxation of the magnetization process is exposed in Figure 3.1. Initially, the two spin states $-M_S$ and $+M_S$ are equally populated. As an external magnetic field is applied in the direction of the magnetization axis, a specific state, $-M_S$ is populated, and then, stabilized at the expense of $+M_S$, until it arrives to a saturation point. Relaxation occurs after the field is taken off, as the systems look for thermal equilibrium.

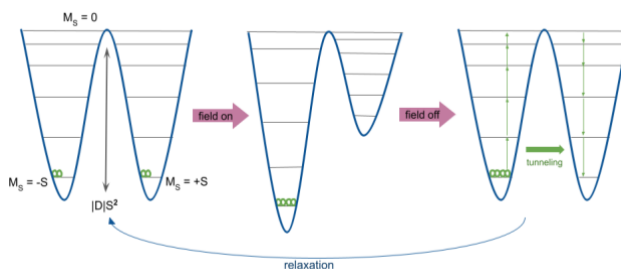


Figure 3.1. Magnetization and magnetic relaxation process of SMMs.¹¹

Based on this model, in order to obtain SMMs with slow relaxation behavior it is necessary to look for molecules with large and negative D value and a large total spin (S).¹² A way to achieve a large total spin is coupling magnetic moments of several metal ions together, but as it has been noticed in other works, increasing S results in very low blocking temperature, probably caused by the fact that D is proportional to $1/S^2$.¹³ Accordingly, increasing the total spin actually reduces anisotropy and the energy barrier does not increase.^{12,14} From an experimental point of view, it is difficult to predict the presence of slow relaxation behavior since the two magnitudes on which it depends cannot be predicted.¹² However, an interesting feature of SMMs is that their anisotropy is determined by the field of the ligand and can be tuned by the choice of such ligands and their coordination geometry.

Nevertheless, there are precedents that demonstrate these properties, which allow us to think that the compounds synthesized in this work may also present them. The focus in this topic has been centered on searching compounds with large magnetic anisotropies. In the recent years, some Co(II) complexes have been reported exhibiting such behaviour.^{15–18}

Mononuclear cobalt(II) complexes have been reported which show slow relaxation of the magnetization. An example is a Co(II) imido complex synthesized by Yao, X.-N. et al. in 2017,¹⁷ which presents a record of the relaxation barrier known for first row transition metals. This work also shows the important role of nitrogen bonds environment in terms of increasing anisotropy. However, in general aspects, their energetic barrier is below what it would be desirable. A promising solution comes from magnetic coupling of metal centers.¹³ As discussed in a more recent work, R. Diego, et al. in 2019⁷ synthesized a Co(II) dinuclear helicate looking for a slow magnetic relaxation in an intermediate geometry between trigonal prism and trigonal antiprism.

In the literature, it is found that Co(II) is a suitable candidate to synthesize SMM since bears up to three unpaired electrons ($S = 3/2$) and its complexes have their record of magnetic anisotropy among the first row metals.^{6,13,17} However, regarding geometry, the literature reports a variety of coordination numbers and geometries for Co(II), but there are few examples of hexacoordinated ones. From these few articles, a distortion of the geometry can be highlighted, as can be seen in the work from R. Diego, et al. (2019).¹⁸⁻²⁰

The objective of the present work is to hold a novel dinuclear Co(II) triple stranded helicate based on previous helicates synthesized by the GMMF research group.²¹ Based on previous studies, a slow relaxation behavior can be expected, as well as a distortion of octahedral geometry of the metal centers in favor of their magnetic properties.

3.2 SPIN CROSSOVER

Apart from the SMM character, there are further possible magnetic properties in the functional molecules that are worth studying. In the last two decades spin crossover compounds (SCO) have been thoroughly researched, although efforts have focused on iron(II) based compounds, whereas Co(II) compounds have been relegated to the background, and only few in-depth studies have been made.²²

SCO in a coordination compound consists of a transition between usually two different spin multiplicities, named low spin (LS) and high spin (HS), in a coordination compound, caused by an external stimuli such as changes of temperature, pressure, magnetic field or light.²³

Our study will be focused on Co(II) spin-transition in an octahedral environment. In such d^7 systems, the d orbitals of the metal split into t_{2g} and e_g subsets. The distribution of electrons over the orbitals is determined by the competition of the ligand field splitting energy Δ and the spin pairing repulsion P . Depending on the species surroundings the strength of the ligand field can

be tuned in favor of SCO. Thus, to observe a SCO, energetically close states Δ will be required, so a quantitative transition of spins to e_g subshell, when an external stimulus occurs, can be achieved.

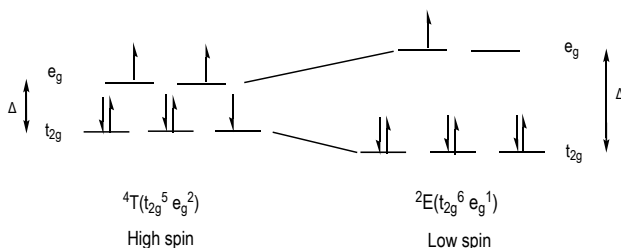


Figure 3.2 Scheme of the electrons distribution over the orbitals of Co(II) in an octahedral environment.

Representation of both possible spin states. Figure generated with *ChemDraw*.

Hence, as can be seen in Figure 3.2, in d^7 octahedral systems the transition switches between the ${}^2E(t_{2g}^6 e_g^1)$ state, which will correspond to LS, and the ${}^4T(t_{2g}^5 e_g^2)$ state, the HS state. Such transition undergoes structural and magnetic changes that can be followed by techniques such as temperature dependence magnetic susceptibility or crystal structure measurements.²² In case of cobalt (II) complexes, the SCO involves one electron which is transferred to the anti-bonding e_g orbital set in contrast with Fe(II) systems, in which two electrons are involved. Therefore, this leads to a less difference in metal-ligand bond distances changes accompanying SCO.²⁴ Furthermore, the unsymmetrically occupied e_g orbital set in the low-spin state causes a Jahn-Teller distortion, which have been observed to have a dependence on the anisotropy D factor.¹⁴ In the literature, it has been crystallographically described for a 6-nitrogen coordination sphere, showing an elongation of the axial Co-N bond length, with spin transition.^{22,25,26} Such differences involve smaller energy barriers, so reduced stimuli will be required to befall spin crossover.^{3,22} This is also going to influence the shape of transition curves, which in most cases have shown to be gradual.²⁷

Despite knowing the spin state transition usually occurs in a gradual way, hysteresis and abrupt spin transitions may result in forming cooperativity. Many of the magnetic properties lay on intermolecular π - π or hydrogen bonds interactions which transmit structural changes arising from SCO.^{22,25,28} For this reason cooperativity has been intensively researched when synthesizing assemblies looking for magnetic properties.

A brief introduction to the relevant literature of Co(II) complexes displaying spin-crossover will be described below. Since Stoufer et al. in 1961 first prepared a mononuclear cobalt complex using tridentate tris-imine ligand. This kind of coordination sphere, which has also been the basis for further compounds exhibiting SCO.^{23,28,29} Although the majority of SCO compounds are mononuclear, there is a growing interest for the synthesis of dinuclear frameworks since they offer the possibility of going through three different magnetic states [HS-HS], [HS-LS], [LS-LS], and allow us to combine the magnetic properties with the coupling interactions.³⁰ Dinuclear compounds will also allow us to encapsulate different guests that can tune the magnetic properties, as discussed below.

3.3. HOST-GUEST SYSTEMS: LOOKING FOR THE MULTIFUNCTIONALITY

Supramolecular chemistry provides the necessary tools to create self-assembled compounds, which interact through non-covalent interactions such as H-bonds, π π interactions, Van der Waals or other weak interactions. Among self-assembled compounds, helicates are the most popular architectures, mostly because they are very common in biological systems. Also, its potential to design complex structures has driven its thorough research.³¹

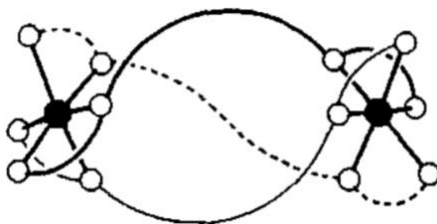


Figure 3.3 Scheme of a triple-stranded helicates.³²

The helicates are formed by ligands that wrap around one or more metallic ions. In order to create such architectures, the choice of ligands is fundamental. Ligands must provide certain flexibility and must be good coordination moieties. The stereochemical preference of the metal ion must be considered to create ligands with matching coordination possibilities. Therefore, for cobalt(II), bidentate ligands will provide an octahedral coordination sphere and a triple-stranded helicate.³² When an helicate is formed, a space between the metal centers is also created, where this cavity has shown an ability to encapsulate guests yielding to interesting host-guest systems. Hence, the template effect looks for the encapsulation of molecules by the choice of appropriate ligands. It has

been observed that the guest molecule can modify the properties of the host molecule or even add more functions.

The literature shows previous examples in which a guest molecule is introduced into a system to combine different properties, either SCO or slow relaxation of magnetization. In particular, the GMMF group has described a family of ligands that are able to form host-guest systems and whose assemblies have achieved good results in this area. They were also able to encapsulate bigger guests. For example Darawsheh, M. et. al. in 2018⁸ describe the encapsulation of a single molecular magnet, $[\text{Cr}^{\text{III}}(\text{Ox})_3]^{3-}$, within an iron(II) helicate with SCO, which set a great example for creation of multifunctional systems. Moreover, they studied the effect of different guests over the host properties.²¹

4. OBJECTIVES

The aims of this project were:

- The design and synthesis of new supramolecular Cobalt(II) dinuclear helicates, to encapsulate anions such as PF_6^- , BF_4^- or ClO_4^- .
- The study of the magnetic behavior of the helicates.
- The characterization of the helicates by single-crystal X-ray diffraction, infrared spectroscopy mass spectrometry and ^{19}F -NMR.

5. EXPERIMENTAL SECTION

5.1. MATERIALS AND METHODS

5.1.1. Infrared Spectroscopy

IR spectra were recorded using Nicolet 6700 FT-IR spectrometer (ALPHA's Platinum ATR single reflection), 4000–400 cm^{-1} range.

5.1.2. Mass Spectrometry

Positive-ion ESI mass spectra were recorded by using a LC/MSD-TOF (Agilent Technologies) with a dual source equipped with a lock spray for reference introduction, at the Unitat d'Espectrometria de Masses (SSR) from the Universitat de Barcelona.

Positive-ion MALDI (Matrix Assisted Laser Deposition Ionization) MS were performed by using a 4800Plus MALDI TOP/TOF (ABSciex-2010) instrument at the Unitat d'Espectrometria de Masses (SSR) from the Universitat de Barcelona, on MeOH/DMSO solutions. The ionization source was MALDI Solid State Laser (Nd:YAG, 355nm, 200Hz, 3-7ns pulse). The analyzer was a TOF/TOF (Time-of Flight) in reflector mode.

5.1.3. Single-Crystal X-ray diffraction

Diffraction data for **1** was collected with a MD2M-Maatel diffractometer at the XALOC beamline at ALBA Synchrotron. Data for compound **3** was collected using a Bruker APEX II CCD diffractometer on the Advanced Light Source beamline 11.3.1 at Lawrence Berkeley National Laboratory, from a silicon 111 monochromator ($\lambda = 0.7749 \text{ \AA}$). Data for compound **2** was collected on a Bruker APEX II QUAZAR diffractometer equipped with a microfocus multilayer monochromator with MoK α radiation ($\lambda = 0.71073 \text{ \AA}$) at the Group of Magnetism and Functional Molecules (GMMF) at the University of Barcelona. Data reduction and absorption corrections were performed by using SAINT and SADABS, respectively. The structures were solved using SHELXT and refined with full-matrix least-squares on F2 by using SHELXL-2014.

5.1.4. ^{19}F NMR Spectroscopy

^{19}F NMR spectra was recorded with Bruker (500 MHz) spectrometer, at 298 K using DMSO- d_6 , located at the the Serveis Científic-Tècnics of the UB.

5.1.5. Magnetic measurements

Variable-temperature magnetic susceptibility data were obtained with a MPMS-XL SQUID magnetometer at the Unitat de Mesures Magnètiques of the Universitat de Barcelona.

5.2. SYNTHESIS OF METALLOCOMPLEXES

5.2.1. Synthesis of $\text{ClO}_4@[\text{Co}_2(\text{L2})_3](\text{ClO}_4)_2(\text{CH}_3\text{O})\cdot n\text{CH}_3\text{OH}$ (1)

A solution of $\text{Co}(\text{ClO}_4)_2\cdot 6\text{H}_2\text{O}$ (11 mg, 0.030 mmol) in methanol (5mL) was prepared and added into a beaker. Under stirring, a solution previously homogenized L2 (20 mg, 0.045 mmol) in methanol (10 mL) was added dropwise. A color change from light red (from the Co solution) to yellow was observed and the solution become cloudy. After stirring the solution for 30 min at room temperature, the solution was filtered with a nylon membrane 0,2 μm pore size.

A solution of TBAClO_4 (20.6 mg, 0.060 mmol) in 5 mL of methanol was prepared and added dropwise to the previously filtered solution. Then it was left stirring for 15 more min, and filtered with a nylon membrane of 0,2 μm pore size.

The crystallization was carried out by it by liquid-liquid diffusion in diethyl ether using a pyrex 15 tube.

This compound was secluded as orange crystals after two weeks, were obtained 1,3 mg. Yield(%): 5%. IR: 3139 (*b* -N-H), 1616 (*b* N-H), 1582(*s* C=C), 1444 (*s* C=C), 1087 (*s* Cl-O), 780 (*b* C-H) cm^{-1} .^{33,34}

5.2.2. Synthesis of $\text{ClO}_4@[\text{Co}_2(\text{L3})_3](\text{ClO}_4)_2(\text{CH}_3\text{O})\cdot n\text{CH}_3\text{OH}$ (2)

A solution of $\text{Co}(\text{ClO}_4)_2\cdot 6\text{H}_2\text{O}$ (10 mg, 0.027 mmol) in methanol (5mL) was prepared and added into a beaker. Under stirring, a solution previously homogenized (20 mg, 0.043 mmol) of L3 in methanol (10 mL) was added dropwise. It was observed a change of color from light red (from the Co solution) to a yellow cloudy solution. After stirring the solution for 30 min at room temperature, the solution was filtered with a nylon membrane of 0,2 μm pore size.

A solution of TBAClO_4 (19,4 mg, 0.056 mmol) in 5 mL of methanol was prepared and added dropwise to the previously filtered solution. Then it was left stirring for 30 more min, and filtered with a nylon membrane of 0,2 μm pore size.

The crystallization was carried out by vapor diffusion in diethyl ether.

This compound was secluded as orange crystals after two weeks, 6.8 mg. Yield(%): 26%. IR: 2362 (*s* C-H), 1622 (*b* -N-H), 1569 (*s* C=C), 1436 (*s* C=C), 1083 (*s* Cl-O), 796 (*b* C-H), 699 (*s* Cl-O) cm^{-1} .^{33,34}

5.2.3. Synthesis of $\text{SiF}_6@[\text{Co}_2(\text{L1})(\text{L3})_2](\text{PF}_6)_2$ (3)

5.2.3.1. Attempt of synthesizing $\text{PF}_6@[\text{Co}_2(\text{L1})(\text{L3})_2](\text{PF}_6)_3$

A solution of $\text{Co}(\text{BF}_4)_2 \cdot 6\text{H}_2\text{O}$ (14.6 mg, 0.042 mmol) in methanol (5 mL) was prepared and added into a beaker. Under stirring, it was added dropwise a solution previously homogenized of L1 (7.8 mg, 0.021 mmol) and (20 mg, 0.042 mmol) of L3 in methanol (10 mL). It was observed a change of color from light red (from the Co solution) to a yellow cloudy solution. After stirring the solution for 30 min at room temperature, the solution was filtered with a nylon membrane of 0,2 μm pore size.

A solution of TBAPF_6 (33.2 mg, 0.086 mmol) in 5 mL of methanol was prepared and added dropwise to the previously filtered solution. Then it was left stirring for 30 more min, and filtered with a nylon membrane of 0,2 μm pore size

Afterwards it was proceeded to do crystallization by liquid-liquid diffusion in toluene using a pyrex 15 tube.

5.2.3.2. Attempt of synthesizing $\text{BF}_4@[\text{Co}_2(\text{L1})_2(\text{L3})](\text{BF}_4)_3$

A solution of $\text{Co}(\text{BF}_4)_2 \cdot 6\text{H}_2\text{O}$ (14.5 mg, 0.042 mmol) in methanol (5mL) was prepared and added into a beaker. While stirring, it was added dropwise a solution previously homogenized of L1 (15.5 mg, 0.042 mmol) and (10 mg, 0.021 mmol) of L3 in methanol (10 mL). It was observed a change of color from light red (from the Co solution) to a yellow cloudy solution. After stirring the solution for 30 min at room temperature, the solution was filtered with a nylon membrane of 0,2 μm pore size.

A solution of TBABF_4 (35.1 mg, 0.107 mmol) in 5 mL of methanol was prepared and added dropwise to the previously filtered solution. Then it was left stirring for 30 more min, and filtered with of 0,2 μm pore size.

Afterwards it was proceeded crystallize by slow evaporation.

The abovementioned procedures were made in order to synthesize $\text{PF}_6@[\text{Co}_2(\text{L1})(\text{L3})_2](\text{PF}_6)_3$ and $\text{BF}_4@[\text{Co}_2(\text{L1})_2(\text{L3})](\text{BF}_4)_3$ compounds, but as characterization have demonstrated, both compounds have not been obtained, it has been obtained $\text{SiF}_6@[\text{Co}_2(\text{L})(\text{L3})_2](\text{PF}_6)_2$ instead. This heteroleptic system was obtained as orange crystals after three weeks, 12.7 mg. Yield(%): 41%.

IR: 3151 (s N-H), 1623 (b -N-H), 1566 (s C=C), 1438 (s C=C), 837 (s P-F), 781 (s Si-F), 697 (s Si-F) cm^{-1} ,^{33,34}

6. SYNTHESIS DISCUSSION

The present describes our attempts to synthesize a novel family of cobalt(II) triple-stranded helicates featuring interesting magnetic properties. In addition, a guest molecule was added, therefore template effect can be tested. This helps us to understand better the template effect, while looking for multifunctionality.

The synthesis is based on a self-assembly process, where a recognition between the components takes place spontaneously to create supramolecular architectures. Furthermore, it is look for structures which can show template effect.

The ligands used differ on its length by a 1,3-bound phenyl rings within the chain, therefore by playing with the ratio of ligands different size cavities can be achieved. This is important because the choice of ligands is fundamental in the design of these systems. Moreover, used ligands, shown in Figure 3.3, not only provide a proper Δ for SCO, but can stabilize guests. Pyridine and pyrazole moieties establish an octahedral environment around the cobalt ions, and possess two extra donor atoms that can form H-bonds with the guest, and a system of aromatic rings that enhance the encapsulation. Furthermore, their interest relies on the increase of cooperativity by linking both metal centers and increasing the formation of π - π interactions because of the aromatic rings. And as it will be seen, these ligands will allow us to encapsulate relatively big anions such as SiF_6^{2-} or ClO_4^- .

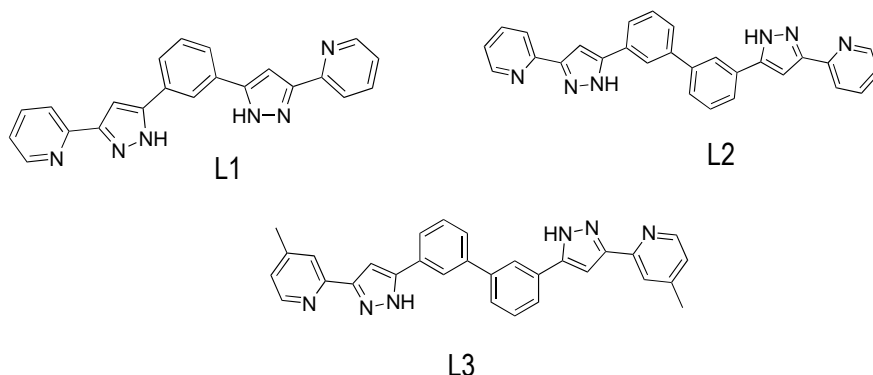


Figure 3.3 Representation of ligands used. **L1**: 1,3-bis(3-(pyridin-2-yl)-1H-pyrazol-5-yl)benzene. **L2**: 3,3'-bis(3-(pyridin-2-yl)-1H-pyrazol-5-yl)-1,1'-biphenyl. **L3**: 3,3'-bis(3-(4-methylpyridin-2-yl)-1H-pyrazol-5-yl)-1,1'-biphenyl. Figure generated with *ChemDraw*.

Compounds **1** and **2** were able to encapsulate a bigger guest, ClO_4^- since they both contain 3 long ligands, either **L2** or **L3**. The chosen ligands revealed that in terms of crystallization **L3** have shown better results than **L2**. There were tried various systems where it was used **L2** instead of **L3**, but L2-based systems did not show reproducibility. From a structural and reactivity point of view, these two can be compared since they have the same length and torsion capacities and can be interchanged without affecting the host of the guest. Unlike **L2** ligand, **L3** has a methyl group in the para position of N atoms from pyridine moieties, which enhances the donor ability of the nitrogen, and the formation of the assembly is therefore favored.

As it was mentioned before in section 5.2.3, the aim of the reaction was to synthesize two different helicates by playing with the proportion of ligands to create different size cavities. The scope was to create different heteroleptic host-guest systems where the guest was BF_4^- or PF_6^- . Therefore, the $\text{SiF}_6@[\text{Co}_2(\text{L1})(\text{L3})_2](\text{PF}_6)_2 \cdot n\text{CH}_3\text{OH}$ was the compound obtained and it comes from the procedure taken to prepare $\text{PF}_6@[\text{Co}_2(\text{L1})(\text{L3})_2]^{3-}$ and $\text{BF}_4@[\text{Co}_2(\text{L1})_2(\text{L3})]^{3-}$ (Sections 5.2.3.1 and 5.2.3.2). This new heteroleptic compound has a counteranion with two negative charges, the SiF_6^{2-} , despite not having introduced silicate in the reagents. The main hypothesis is that this silicate comes from the glass material used during the crystallization. Thus, the heteroleptic helicate is so stabilized by this guest that can tear off the Si of the glass.

To synthesize an assembly where BF_4^- , a smaller molecule, is encapsulated, the ratio of ligands **L1**:**L3** required is 2:1, then having two short ligands (**L1**) and one long (**L3**). This ratio creates a smaller cavity unlikely to encapsulate octahedral molecules such as PF_6^- or SiF_6^{2-} . Moreover, to

ensure the encapsulation of BF_4^- , it was added in excess. However, regardless of all experiments, when having an heteroleptic system no matter the amount of reagents, it is formed $\text{SiF}_6@[\text{Co}_2(\text{L1})(\text{L3})_2](\text{PF}_6)_2$. Hence, it has been seen an enormous template effect to form the specie where SiF_6^{2-} anion is encapsulated. Structural parameters permitted to observe the different bond distances from the guest and the counterions (as it will be further will be explained). Also, they allowed to make a comparison between the guest's Si-F bond distances and the counterions P-F bond distances. Furthermore, from IR spectroscopy (Appendix 1, Figure A1.3) it could be seen a band at 680 cm^{-1} and at 781 cm^{-1} corresponding to reported stretching bands from Si-F.³⁵

Thus, in the future, to get the effective encapsulation of PF_6^- or BF_4^- any source of silicon will need to be removed, and work with plastic material.

7. CRYSTAL STRUCTURES

The X-ray diffraction measures were performed at 100K and we were able to successfully solve the structures for compounds **1**, **2** and **3**.

7.1. CRYSTAL STRUCTURE OF $\text{ClO}_4@[\text{Co}_2(\text{L2})_3](\text{ClO}_4)(\text{OH})(\text{CH}_3\text{O})\cdot n\text{CH}_3\text{OH}$ (**1**)

Compound **1** was prepared from the reaction of $\text{Co}(\text{ClO}_4)_2\cdot 6\text{H}_2\text{O}$ with L2 in methanol. Then, an excess of TBAClO_4 in methanol was added to provide the counteranions and the guest molecules. Finally, orange crystals are obtained by liquid-liquid diffusion with diethyl ether.

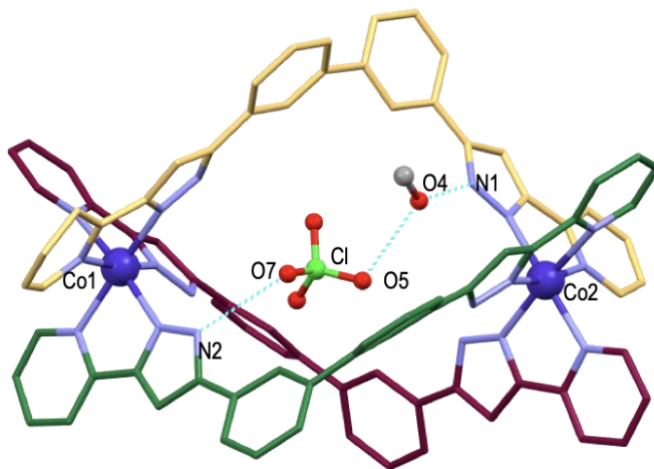


Figure 7.1 Molecular representation of cation $\text{ClO}_4@[\text{Co}_2(\text{L}2)_3](\text{CH}_3\text{O})^{2+}$ of **1**. It shows the encapsulation of ClO_4^- and the most important H bonds. The structure could not be completely refined, therefore H do not appear. Solvent molecules and counteranions are omitted for better sight. The Co(II) centers are shown in blue and N in light blue, Cl in light green, and ligands **L2** in yellow, purple and dark green.

The structure is not fully refined, therefore the hydrogen atoms forming H-bonds with guest, are not shown. However, the H-bonds established can be deduced hence are shown in Figure 7.1. The ligands **L2** wrap around the cobalt ions to form a triple-stranded helicate, conferring the cobalt centers an octahedral coordination through the pyrazole and pyridine moieties with Co-N bonds ranging 2.1033 to 2.1798 Å, which are typical for HS state.²⁷ Biphenyls confer the helicate more flexibility to accomplish such structure and when coordinated they experience a torsion. Thus, the use of larger ligands with certain flexibility allows the helicate to hold bigger guests.

Compound **1** crystallizes in the monoclinic $P 2_1/c$ space group and the unit cell encloses three assemblies. Apart from the cationic specie $\text{ClO}_4@[\text{Co}_2(\text{L}2)_3]^{3+}$ it is observed as counterions a molecule of ClO_4^- and clearly OH^- ions and a CH_3O^- . As seen in Figure 7.1, the ClO_4^- it is found to be held within the cavity created by the three ligands through H-bond interaction from the pyrazole groups. An H-bond is directly established between nitrogen N2 and O7 with a distance of 2.903 Å, another H-bond have formed between the pyrazole group and a methanol group located among the ligand and the guest. As well, the guest is located in a non-symmetrical position of the cavity, more proximate to one of the cobalt atoms [$\text{Co}1 \cdots \text{Cl}2 = 5.2161$ Å, $\text{Co}2 \cdots \text{Cl}2 = 1.1241$ Å].

Compound	$\text{ClO}_4@[\text{Co}_2(\text{L}_2)_3](\text{ClO}_4)(\text{OH})(\text{CH}_3\text{O})$
Compound	$\text{ClO}_4@[\text{Co}_2(\text{L}_2)_3](\text{ClO}_4)(\text{OH})(\text{CH}_3\text{O})$
Formula	$\text{C}_{84}\text{H}_{60}\text{N}_{18}\text{Co}_2\text{ClO}_4$
T(K)	100
Crystal system	monoclinic
Space group	$P 2_1/c$
a [Å]	22.7364(3)
b [Å]	18.4080(2)
c [Å]	27.0501(3)
α [°]	90
β [°]	93.783(1)
γ [°]	90
Cell Volume [Å ³]	11296.7

Table 7.1 Crystallographic data and parameters for 1.

Atoms	Distance [Å]	Bond	Distance [Å]	Bond	Distance [Å]
Co01-NC	2.1113	Co02-NB	2.1555	Cl1-O3	1.3623
Co01-ND	2.1063	Co02-NH	2.1241	Cl1-O4	1.3382
Co01-NQ	2.1628	Co02-NJ	2.1624	Cl2-O5	1.3078
Co01-NR	2.1374	Co02-NO	2.1033	Cl2-O6	1.3213
Co01-NU	2.1401	Co02-N8	2.1246	Cl2-O7	1.3733
Co01-N7	2.1200	Cl1-O1	1.3867	Cl2-O8	1.3102
Co02-NA	2.1798	Cl1-O2	1.4158	N1- H...O4...O5	2.8115/2.8629
				N2-H...O7	2.903

Table 7.2 Selected bond distance values for 1.

7.2. CRYSTAL STRUCTURE OF $\text{ClO}_4@[\text{Co}_2(\text{L}_3)_3](\text{ClO}_4)_2(\text{CH}_3\text{O}) \cdot n\text{CH}_3\text{OH}$ (2)

Compound **2** was prepared from the reaction of $\text{Co}(\text{ClO}_4)_2 \cdot 6\text{H}_2\text{O}$ with **L3** in methanol, giving an homoleptic structure. Then, an excess of TBAClO_4 in methanol was added to provide the

counterions and the guest molecules. Finally, orange crystals are obtained by vapor diffusion with diethyl ether.

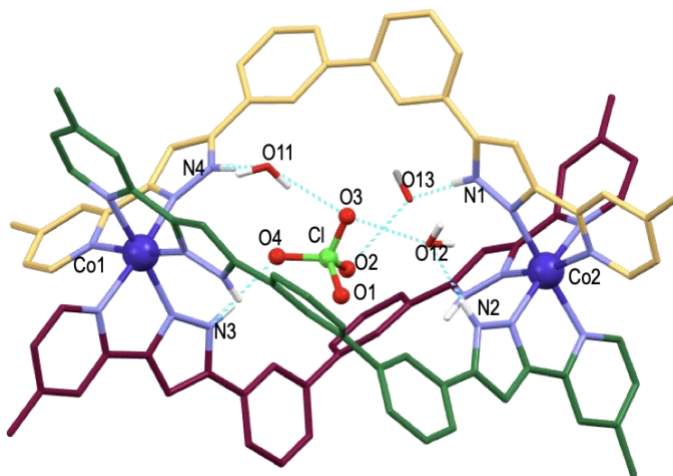


Figure 7.2 Molecular representation of cation $\text{ClO}_4@[\text{Co}_2(\text{L}_3)_3](\text{CH}_3\text{O})_2^{2+}$ of **2**. It shows the encapsulation of ClO_4^- and the H bonds. Solvent molecules and counteranions are omitted for better sight. The Co(II) centers are shown in blue and N in light blue, O in red, Cl in light green, and ligands L3 in yellow, purple and dark green.

Compound **3** belongs to the monoclinic $P 2_1/n$ space group. The cation $\text{ClO}_4@[\text{Co}_2(\text{L}_3)_3]^{3+}$ is formed by three ligands **L3**, which are connected to the Co(II) by the nitrogen atoms of pyridine and pyrazole groups, providing them an octahedral environment. The average distances for Co1-N and Co2-N are respectively 2.130 Å and 2.121 Å, the typical length for a HS state cobalt (II).²⁷

As seen in Figure 7.2 the host-guest recognition takes place through four hydrogen bonds. Showing to be stronger the ones near the Co1, since are formed directly by the NH groups of ligand **L3**. On the other hand, the interactions established near the Co2 are done through two water molecules and a CH_3O^- molecule. This evidences the displacement of the guest from the center of the cavity as it can be seen in the length of the guest's distance from the cobalt ions [Co1-Cl = 5.2723 Å, Co2-Cl = 6.1096 Å].

As counterions, two ClO_4^- and a methoxide ion are presented and, as it was explained before, two molecules of water. In addition, methanol molecules were disordered within the lattice providing the structure hydrogen bonds keeping the different helicates connected.

Compound	ClO₄@[Co₂(L3)₃](ClO₄)₂(CH₃O)
Formula	C ₉₀ H ₇₂ N ₁₈ ClCo ₂ O ₄
T(K)	100
Crystal system	monoclinic
Space group	P 2 ₁ /n
a [Å]	22.968(1)
b [Å]	18.0371(9)
c [Å]	27.1563(12)
α [°]	90
β [°]	94.962(2)
γ [°]	90
Cell Volume [Å ³]	11208.1

Table 7.3 Crystallographic data and parameters for **2**.

Atoms	Distance [Å]	Bond	Distance [Å]	Bond	Distance [Å]
Co1-N7	2.1370	Co2-NM	2.0988	N1- H...O13...O2	2.7665/2.7573
Co1-N8	2.0771	Co2-NO	2.0904	N4- H...O11...O3	2.7497/2.9566
Co1-N9	2.1709	Co2-NR	2.1316	N2- H...O12...O3	2.7844/2.9718
Co1-NB	2.1300	Co2-N1B	2.1450	N3-H...O4	2.8576
Co1-NF	2.1454	Cl-O4	1.427	Co1-Cl	5.2723
Co1-NG	2.1222	Cl-O3	1.3696	Co2-Cl	6.1096
Co2-NH	2.1545	Cl-O1	1.4113		
Co2-NJ	2.1081	Cl-O2	1.4068		

Table 7.4 Selected bond distance values for **2**.

7.3. CRYSTAL STRUCTURE OF $\text{SiF}_6@[\text{Co}_2(\text{L}1)(\text{L}3)_2](\text{PF}_6)_2 \cdot n\text{CH}_3\text{OH}$ (**3**)

Thanks to X-ray diffraction studies, it was determined that compound **3** crystallizes in a monoclinic $C c$ space group. Ligands **L1** and **L3** wrap around the cobalt ions conferring an octahedral environment. Since the ratio of **L1** and **L3** is 1:2 a bigger cavity is formed, which is able to encapsulate octahedral anions, such as SiF_6^{2-} . As counterions, two PF_6^- are observed. The nature of these two anions is evidenced by the P-F bond distances, which is in average 1.570 Å, corresponding to PF_6^- ions.

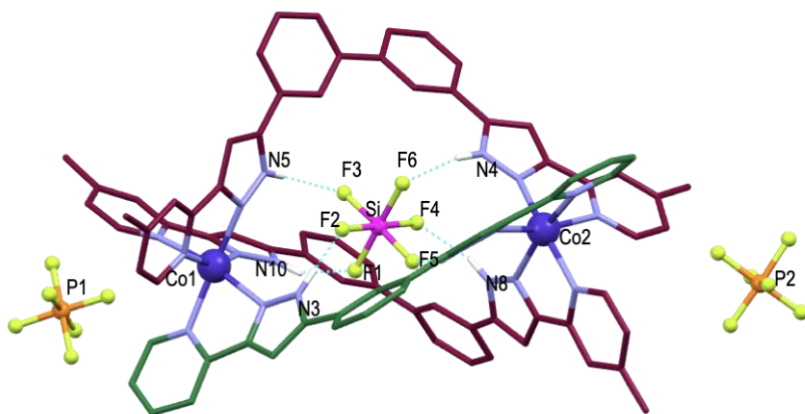


Figure 7.3 Molecular representation of the heteroleptic compound $\text{SiF}_6@[\text{Co}_2(\text{L}1)(\text{L}3)_2](\text{PF}_6)_2$ of **3**. It shows the encapsulation of SiF_6^{2-} . Solvent molecules are omitted for better sight. The Co(II) centers are shown in blue and N in light blue, F in yellow, P in orange, Si in pink and ligands **L3** purple and **L1** in dark green.

Structural parameters permitted us to determine the bond distances for the SiF_6^{2-} encapsulated anion and compare it with the counterions PF_6^- bond distances. This gives the first prove of the encapsulation of an unexpected anion. Bond distances showed to be significantly different for the guest SiF_6^{2-} (1.691 Å) and for the counter ions PF_6^- (1.570 Å). The guest's distances were compared with reported ones and showed to be consistent with the Si-F bond distance reported value of 1.680 Å from Ouasri A. et al. (2003).³⁵ Moreover, this is also consistent with the presence of two counterions, since SiF_6^{2-} possess two negative charges, two PF_6^- ions will be required to offset the helicate charge. As well it is noticed that the Si-Co distances are 5.221 and 5.219 Å, then the guest stays centered inside the cavity.

Compound	SiF₆@[Co₂(L1)(L3)₂](PF₆)₂
Formula	C ₈₂ H ₆₄ N ₁₈ Co ₂ PF ₆
T(K)	100
Crystal system	monoclínic
Space group	C c
a [Å]	22.6317(9)
b [Å]	26.9437(11)
c [Å]	17.9074(7)
α [°]	90
β [°]	126.420
γ [°]	90
Cell Volume [Å ³]	8786.86

Table 7.5 Crystallographic data and parameters for **3**.

Atoms	Distance [Å]	Bond	Distance [Å]	Atoms	Distance [Å]
Co1-N1	2.1727	Si-F1	1.7029	P2-F12	1.6032
Co1-N1A	2.1444	Si-F2	1.6858	Co1-Si	5.221
Co1-N2	2.1330	Si-F3	1.6710	Co2-Si	5.219
Co1-N2A	2.1253	Si-F4	1.6751		
Co-N12	2.0996	Si-F5	1.7169		
Co-N5	2.1561	Si-F6	1.6949		
Co-N5A	2.1131	P2-F7	1.5571		
Co2-N6	2.1241	P2-F8	1.5356		
Co2-N6A	2.1717	P2-F9	1.5599		
Co2-N7	2.1544	P2-F10	1.6211		
Co2-N9	2.1355	P2-F11	1.5972		

Table 7.6 Bond distance values for **3**.

8. ^{19}F NMR SPECTROSCOPY

To pre-examine the nature of the encapsulated specie and the counterions in the compound **3**, a ^{19}F NMR spectrum was recorded. Two different important signals were sought, the fluoride coming from the encapsulated molecule SiF_6^{2-} and the fluoride from counterions PF_6^- . In Figure 8.1 these two different signals can be clearly observed. At -71 ppm appears a sharp doublet of the PF_6^- arising from the ^{19}F - ^{31}P coupling ($J = 755.5 \text{ Hz}$).³⁶ Moreover, it is observed a signal at -134 ppm due to the SiF_6^{2-} .³⁷ Therefore, the encapsulation of SiF_6^{2-} is again confirmed. The doublet over the -148 ppm is consistent with the presence of some tetrafluoroborate, which presents scalar coupling of both isotopes ^{11}B and ^{10}B with ^{19}F . This signal may be caused by the presence of starting material ($\text{Co}(\text{BF}_4)_2$ contained in mother liquors) which indicates an inappropriate treatment of the crystalline sample before characterization. Besides it is observed a signal at -108 ppm that can be caused by the hydrolysis of PF_6^- , forming PF_2O_2 .³⁸

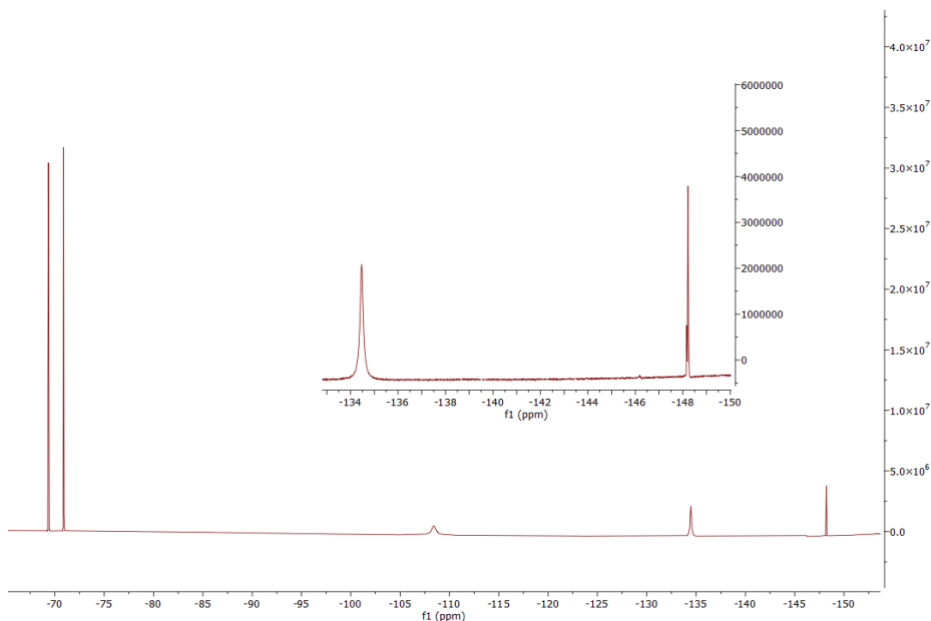


Figure 8.1 ^{19}F NMR for compound **3** recorded at 500 MHz in DMSO. In the inserted there is an expansion of region between -130 and -150 ppm.

9. MASS SPECTROMETRY

ESI Positive-ion ESI were performed for compounds **1**, **2** and **3**. Since only the ligands could be seen no further information could be obtained by this technique. Therefore it was decided to perform a Positive-ion MALDI in solution of DMSO:MeOH (1:1). The results obtained are not clear and do not adjust to calculated values (calculated with the program *Prot-Pi Mass Spectrum Simulator*). The cation intensity it is very diluted, and the isotopic distribution is unclear. The same happens for compound **3**. For this reason the Positive-ion MALDI spectrometry must be repeated, in this case in solid state. The Appendix 2 shows the results obtained for MALDI-TOF.

10. MAGNETIC PROPERTIES

The compounds have been magnetically studied by the temperature dependent magnetic susceptibility, plotting $\chi_m T$ versus temperature T, where χ_m is the molar magnetic susceptibility. Usually, for compounds showing spin transition give a curve with an abrupt or gradual increasing from small values of $\chi_m T$ to bigger ones, and ideally two plateaus are expected, one for each spin state in which the compound goes through. To determine the theoretical values for magnetic susceptibility it has been used the following equations:

$$\chi_m = \chi_p \cdot \chi_d$$

$$\mu = \sqrt{n(n+2)}$$

$$\mu = \sqrt{8 \cdot \chi_p \cdot T}$$

As well it was studied the its magnetic susceptibility in a range of frequencies and at different fields to observe if once a magnetic field is applied it can be retained. If this is observed it could be confirmed the SMM behavior. For this, it is expected to see a gradual increase over X'' versus frequency plot, until reaching a maximum and then a slow descent for each of the fields applied.

10.1. MAGNETIC MEASUREMENTS FOR $\text{Co}_4@[\text{Co}_2(\text{L}3)_3][(\text{ClO}_4)_2(\text{CH}_3\text{O})\cdot n\text{CH}_3\text{OH}$ (**2**)

Magnetic susceptibility data of compound **2** were carried out in a temperature range of 2 – 300 K under an applied field of 1kOe. The plot is shown in Figure 10.1, where it can be seen a gradual increase until at a $\chi_m T$ value of 5.6 $\text{emu}\cdot\text{mol}^{-1}\cdot\text{K}$ which differs from the theoretical value ions of 3.2 $\text{emu}\cdot\text{mol}^{-1}\cdot\text{K}$ calculated for two no-interacting Co(II). Similar values have been reported and can be rationalized by the spin-orbit coupling.⁷ LS state is not reached at any range of temperatures ($\chi_m T$ value for a LS: 0.7 $\text{emu}\cdot\text{mol}^{-1}\cdot\text{K}$) so it can be said that for the entire range of temperatures the system stays in HS.

As no transition occurs it can be concluded that compound **2** does not present SCO. The shift that is observed at 20 K (Figure 10.1 right graph) can be explained by the phenomenon of spin canting. This is a behavior that arises from the single-molecular magnet anisotropy, and is caused by the defect of the magnetic moments from the orientation plane. Despite it is a relatively common phenomenon, when it comes to cobalt (II) it has been scarcely reported.³⁹

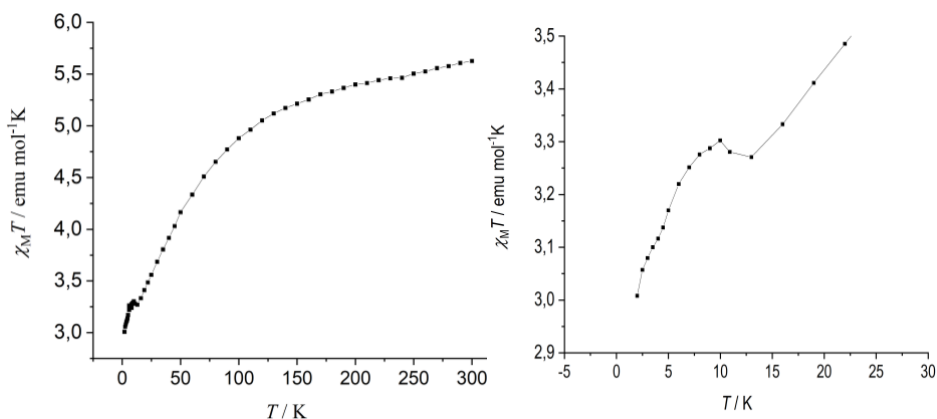


Figure 10.1 Plot of Temperature dependence of $\chi_m T$ for **2**. Right graph is a zoom in of region 0 to 30 K.

This value of magnetic susceptibility at room temperature is typical for a HS cobalt which agrees with the structural parameters. However, the complex does not show spin crossover over the range of temperatures.

AC measurements were carried out, with the aim of study if a slow relaxation of magnetization was presented (Figure 10.2). The measurements were performed at 0G with no substantial

results, then the measurements were taken at a magnetic field of 1000G for which there was a response, but a maximum was not reached. The measurements were carried out at 2 K and varying the magnetic field and χ' and χ'' were plotted against frequencies. Given this results it would be interesting to perform the experiments in the magnetometer equipped with a SQUID sensor and a commercial Physical Properties Measurement System (PPMS) which can achieve up to 10000Hz and may allow to observe the slow relaxation behavior and have already been useful in a similar case.⁷

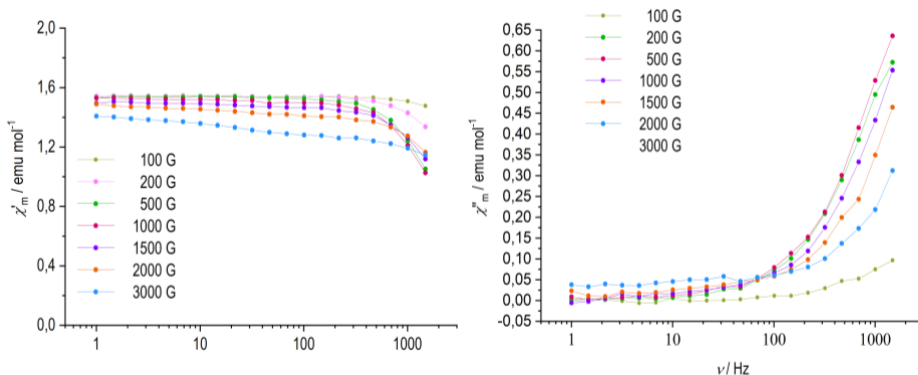


Figure 10.2 In-phase χ' (left) and out-of-phase χ'' (right) ac magnetic susceptibility plot for measured at 2 K for **2**

10.2. MAGNETIC MEASUREMENTS FOR $\text{SiF}_6@[\text{Co}_2(\text{L}1)(\text{L}3)_2](\text{PF}_6)_2$ (**3**)

The magnetic response of compound **3** could also be studied. The plot of the magnetic susceptibility in front of the temperature is shown in Figure 10.3 where it can be observed the HS state over the entire temperature range. Since the expected LS state value of $\chi_m T$ ($0.7 \text{ emu} \cdot \text{mol}^{-1} \cdot \text{K}$) is not reached at any temperature, it is assumed the sole presence of HS state. Then, the difference between the expected at the $\chi_m T$ value of $3.2 \text{ emu} \cdot \text{mol}^{-1} \cdot \text{K}$, and the experimental $\chi_m T$ value of $6.5 \text{ emu} \cdot \text{mol}^{-1} \cdot \text{K}$, is owed to the spin-orbit coupling.⁷ But also, as it was explained in section 8, the ^{19}F NMR shows a magnetic impurity which clearly affects the entire characterization of the compound **3** and the huge difference between the experimental and theoretical values of $\chi_m T$ can be attributed to this as well.

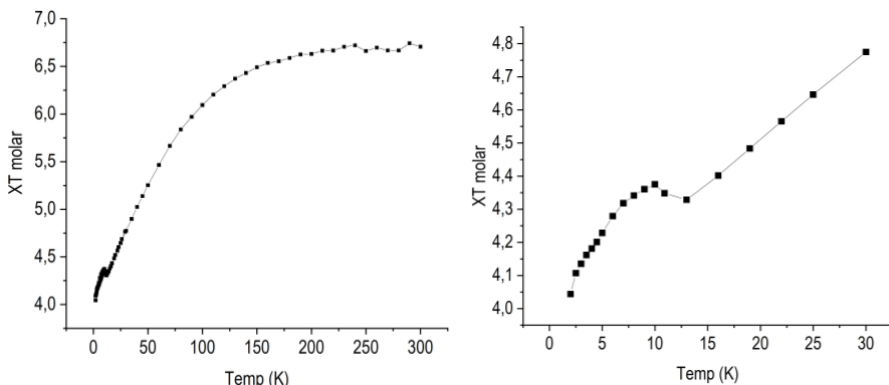


Figure 10.3 Plot of Temperature dependence of $\chi_m T$ for **3**. Right graph is a zoom in of region 0 to 30 K.

As the LS state is not reached, no spin transition occur, thus compound **2** does not present SCO. As in the previous compound it is observed a shift over at low temperature (Figure 10.3, right), over the 20 K, possibly attributed to the spin canting phenomenon.

AC measurements were carried out for compound **3** analogously to the previously described and the magnetic response shows the same trend. In Figure 10.4 is shown the plot of X' and X'' against frequencies where no maximum is evidenced. For this reason, as mentioned above, it would be interesting to carry out the studies at higher frequencies.

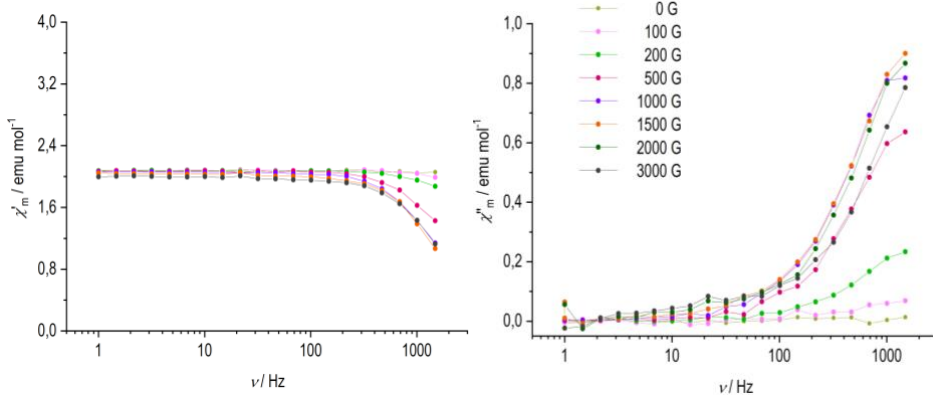


Figure 10.4 In-phase χ' (left) and out-of-phase χ'' (right) ac magnetic susceptibility plot for measured at 2 K for **3**.

To sum up, magnetic studies have revealed that none of the compounds studied presented a SCO behavior, and stay in the entire range of temperatures at HS state agreeing the structural parameters. But both present a shift at low temperatures over the 20 K, which could be explained by the spin canting phenomenon. To ensure the reproducibility of this conduct, the experiments will have to be repeated.

Among the studies in phase and out of phase both compounds show a very similar plot. In none of the cases a maximum is reached but it should be studied at higher frequencies to see its conduct and thus be able to affirm that it presents slow relaxation of the magnetization.

11. CONCLUSIONS

Three novel cobalt (II) complexes were successfully synthesized and a magnetic study could be performed for two of them. Two homoleptic compounds could be synthesized, which allow us to test its different crystallization ability. Furthermore, an heteroleptic compound was prepared, permitting us to better understand the template effect.

Compound **3**, although it was not expected, highlights the enormous template effect of some species, like SiF_6^{2-} . Even when the reagents were introduced in the least favorable proportion, and even when the desired guest was introduced in excess. Based on literature,⁴⁰ it has been hypothesized that silicon comes from glass material used during the synthesis and the heteroleptic systems tears it off from them. Maybe its huge stability is caused because of the two negative charges of the SiF_6^{2-} .

Magnetic measurements revealed that compounds **2** and **3** showed a very similar response, although being different systems (homoleptic and heteroleptic respectively) and holding different guests. Neither of the compounds presented SCO, however, they showed a magnetic response for the study of their slow relaxation of the magnetization, but with no reach of a maximum. Thus, to classify the compounds as SMM it will be required: repeat the magnetic measurements with samples carefully collected in order to avoid magnetic impurities from starting materials and carry out further studies at higher frequencies.

All in all, the new compounds synthesized represent a new family of cobalt (II) complexes with a great potential, which pave the way to keep their study and to research for more functionalities, especially the heteroleptic system, which revealed interesting and unexpected features to in depth study.

12. REFERENCES AND NOTES

1. Piguet, C., Bernardinelli, G. & Hopfgartner, G. Helicates as Versatile Supramolecular Complexes. *Chem. Rev.* 97, 2005–2062 (1997).
2. Lehn, J. M. et al. Spontaneous assembly of double-stranded helicates from oligobipyridine ligands and copper(I) cations: structure of an inorganic double helix. *Proceedings of the National Academy of Sciences* 84, 2565–2569 (1987).
3. Krivokapic, I. et al. Spin-crossover in cobalt(II) imine complexes. *Coordination Chemistry Reviews* vol. 251 364–378 (2007).
4. Bogani, L. & Wernsdorfer, W. Molecular spintronics using single-molecule magnets. *Nature Materials* 7, (2008).
5. Caneschi, A. S. R., Gatteschi, D., Sessoli, R. & Novak, M. A. Magnetic bistability in a metal-ion cluster. *Nature* 365, 141–143 (1993).
6. Aromí, G. & Brechin, E. K. Synthesis of 3d metallic single-molecule magnets. *Structure and Bonding* 122, 1–67 (2006).
7. Diego, R. et al. Coordination [Co^{II}₂] and [Co^{II}Zn^{II}] Helicates Showing Slow Magnetic Relaxation. *Inorganic Chemistry* 58, 9562–9566 (2019).
8. Darawsheh, M., Barrios, L. A., Roubeau, O., Teat, S. J. & Aromí, G. Encapsulation of a Cr III Single-Ion Magnet within an Fe II Spin-Crossover Supramolecular Host. *Angewandte Chemie* 130, 13697–13701 (2018).
9. Aguilà, D. et al. Selective Lanthanide Distribution within a Comprehensive Series of Heterometallic [LnPr] Complexes. *Inorganic Chemistry* 57, 8429–8439 (2018).
10. Bogani, L. & Wernsdorfer, W. Molecular spintronics using single-molecule magnets. *Nanoscience And Technology: A Collection of Reviews from Nature Journals* 7, 179–186 (2010).
11. Neese, F. & Pantazis, D. A. What is not required to make a single molecule magnet. *Faraday Discuss.* 148, 229–238 (2011).
12. Cirera, J., Ruiz, E., Alvarez, S., Neese, F. & Kortus, J. How to build molecules with large magnetic anisotropy. *Chemistry - A European Journal* 15, 4078–4087 (2009).
13. Rechkemmer, Y. et al. A four-coordinate cobalt(II) single-ion magnet with coercivity and a very high energy barrier. *Nature Communications* 7, 1–8 (2016).
14. Gomez-Coca, S., Cremades, E., Aliaga-Alcalde, N. & Ruiz, E. Mononuclear single-molecule magnets: Tailoring the magnetic anisotropy of first-row transition-metal complexes. *Journal of the American Chemical Society* 135, 7010–7018 (2013).
15. Massard, A., Braunstein, P., Danopoulos, A. A., Choua, S. & Rabu, P. Studies on Three-Coordinate [Co(N(SiMe₃)₂)₂L] Complexes, L = N-Heterocyclic Carbene. *Organometallics* 34, 2429–2438 (2015).
16. Novikov, V. v. et al. A Trigonal Prismatic Mononuclear Cobalt(II) Complex Showing Single-Molecule Magnet Behavior. *Journal of the American Chemical Society* 137, 9792–9795 (2015).
17. Yao, X. N. et al. Two-coordinate Co(II) imido complexes as outstanding single-molecule magnets. *Journal of the American Chemical Society* 139, 373–380 (2017).
18. Ozumerzifon, T. J., Bhowmick, I., Spaller, W. C., Rappé, A. K. & Shores, M. P. Toward steric control of guest binding modality: a cationic Co(II) complex exhibiting cation binding and zero-field relaxation. *Chemical Communications* 53, 4211–4214 (2017).
19. Zhang, Y.-Z. et al. Trigonal antiprismatic Co(II) single molecule magnets with large uniaxial anisotropies: importance of Raman and tunneling mechanisms. *Chemical Science* 7, 6519–6527 (2016).
20. Chandrasekhar, V., Dey, A., Mota, A. J. & Colacio, E. Slow Magnetic Relaxation in Co(III)–Co(II) Mixed-Valence Dinuclear Complexes with a Co^{II}O₅X (X = Cl, Br, NO₃) Distorted-Octahedral Coordination Sphere. *Inorganic Chemistry* 52, 4554–4561 (2013).

21. Darawsheh, M. D., Barrios, L. A., Roubeau, O., Teat, S. J. & Aromi, G. Guest-tuned spin crossover in flexible supramolecular assemblies templated by a halide (Cl^- , Br^- or I^-). *Chemical Communications* 53, 569–572 (2017).
22. Goodwin, H. A. Spin Crossover in Cobalt(II) Systems. *Top. Curr. Chem.* 234, 23–47 (2004).
23. Darawsheh, M., Barrios, L. A., Roubeau, O., Teat, S. J. & Aromi, G. Guest-, Light- and Thermally-Modulated Spin Crossover in $[\text{Fe}^{\text{II}}_2]$ Supramolecular Helicates. *Chemistry - A European Journal* 22, 8635–8645 (2016).
24. Hayami, S., Komatsu, Y., Shimizu, T., Kamihata, H. & Lee, Y. H. Spin-crossover in cobalt(II) compounds containing terpyridine and its derivatives. *Coordination Chemistry Reviews* 255, 1981–1990 (2011).
25. Hayami, S., Karim, M. R. & Lee, Y. H. Magnetic behavior and liquid-crystal properties in spin-crossover cobalt(II) compounds with long alkyl chains. *European Journal of Inorganic Chemistry* 683–696 (2013)
26. Kilner, C. A. & Halcrow, M. A. An unusual discontinuity in the thermal spin transition in $[\text{Co}(\text{terpy})_2][\text{BF}_4]_2$. *Dalton Transactions* 39, 9008–9012 (2010).
27. Bhar, K. et al. Crystallographic Evidence for Reversible Symmetry Breaking in a Spin-Crossover d_7 Cobalt(II) Coordination Polymer. *Angewandte Chemie International Edition* 51, 2142–2145 (2012).
28. Craig, G. A., Roubeau, O. & Aromi, G. Spin state switching in 2,6-bis(pyrazol-3-yl)pyridine (3-bpp) based Fe(II) complexes. *Coordination Chemistry Reviews* vol. 269 13–31 (2014).
29. Stoufer, R. C., Busch, D. H. & Hadley, W. B. UNUSUAL MAGNETIC PROPERTIES OF SOME SIX-COORDINATE COBALT(II) COMPLEXES ¹ —ELECTRONIC ISOMERS. *Journal of the American Chemical Society* 83, 3732–3734 (1961).
30. Murray, K. S. Advances in Polynuclear Iron(II), Iron(III) and Cobalt(II) Spin-Crossover Compounds. *European Journal of Inorganic Chemistry* 2008, 3101–3121 (2008).
31. Albrecht, M. "Let's twist again" - Double-stranded, triple-stranded, and circular helicates. *Chemical Reviews* vol. 101 3457–3497 (2001).
32. Williams, A. F., Piquet, C. & Bernardinelli, G. A Self-Assembling Triple-Helical Co(II) Complex : Synthesis and Structure. *Angewandte Chemie International Edition in English* 30, 1490–1492 (1991).
33. Ernö Pretsch, Philippe Bühlmann & Martin Badertscher. *Structure Determination of Organic Compounds.* (Springer Berlin Heidelberg, 2009).
34. Nakamoto, K. *Infrared and Raman Spectra of Inorganic and Coordination Compounds.* (John Wiley & Sons, Inc., 2008).
35. Ouasri, A., Rhandour, A., Dhmelincourt, M.-C., Dhmelincourt, P. & Mazzah, A. The infrared and Raman spectra of ethylammonium hexafluorosilicate $[\text{C}_2\text{H}_5\text{NH}_3]_2\text{SiF}_6$. *Spectrochimica Acta Part A: Molecular and Biomolecular Spectroscopy* 59, 357–362 (2003).
36. Ochoa, G., Pilgrim, C. D., Kerr, J., Augustine, M. P. & Casey, W. H. Aqueous geochemistry at gigapascal pressures: NMR spectroscopy of fluoroborate solutions. *Geochimica et Cosmochimica Acta* 244, 173–181 (2019).
37. Rashidi, N., Vai, A. T., Kuznetsov, V. L., Dilworth, J. R. & Edwards, P. P. Origins of conductivity improvement in fluoride-enhanced silicon doping of ZnO films. *Chemical Communications* 51, 9280–9283 (2015).
38. Ferrer, M. et al. Self-Assembled, Highly Positively Charged, Allyl–Pd Crowns: Cavity-Pocket-Driven Interactions of Fluoroanions. *Chemistry – A European Journal* 26, (2020).
39. Barrios, L. A. et al. Preparation and Structure of Three Solvatomorphs of the Polymer $[\text{Co}(\text{dbm})_2(4\text{ptz})]_n$: Spin Canting Depending on the Supramolecular Organization. *Inorganic Chemistry* 46, 7154–7162 (2007).
40. Sun, M.-Y., Wang, X.-Z., Chen, Z.-Y., Zhou, X.-P. & Li, D. Assembly of Metal–Organic Frameworks of SiF_6^{2-} in Situ Formed from Borosilicate Glass. *Inorganic Chemistry* 58, 12501–12505 (2019).

13. ACRONYMS

D	Magnetic anisotropy
GMMF	Grup de magnetisme i molècules funcionals
HS	High Spin
P	Spin pairing repulsion
S	Spin
SCO	Spin Crossover
SMM	Single molecular magnets
SQUID	Superconducting Quantum Interference Device
LS	Low Spin
L1	1,3-bis(3-(pyridin-2-yl)-1H-pyrazol-5-yl)benzene
L2	3,3'-bis(3-(pyridin-2-yl)-1H-pyrazol-5-yl)-1,1'-biphenyl
L3	3,3'-bis(3-(4-methylpyridin-2-yl)-1H-pyrazol-5-yl)-1,1'-biphenyl
MALDI	Matrix Assisted Laser Deposition Ionization
U_{eff}	Effective energetic barrier
χ^m	Molar Magnetic Susceptibility
Δ	Ligand field splitting energy

APPENDICES

APPENDIX 1: IR SPECTRA

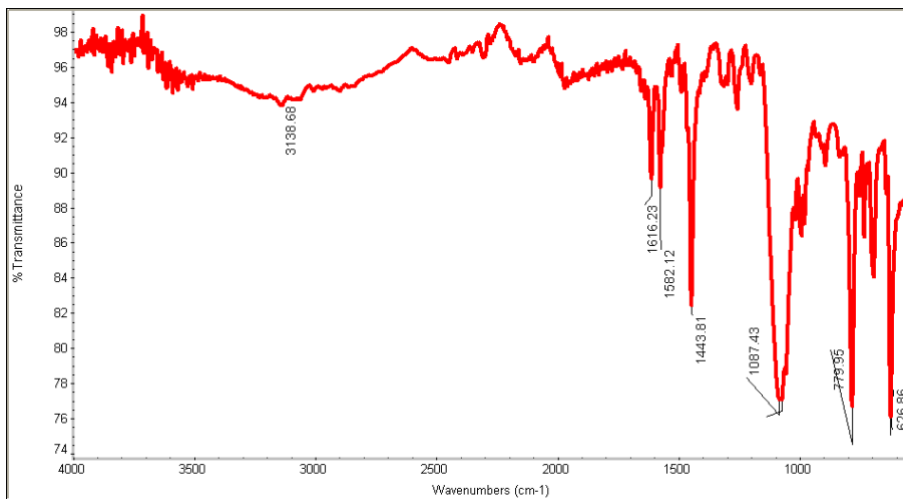


Figure A1.1. IR spectra of 1

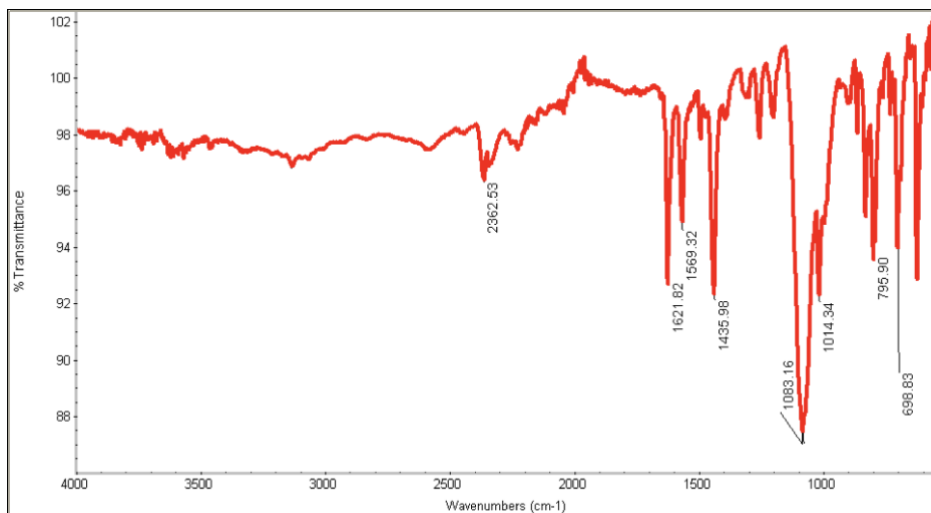


Figure A1.2. IR spectra of 2

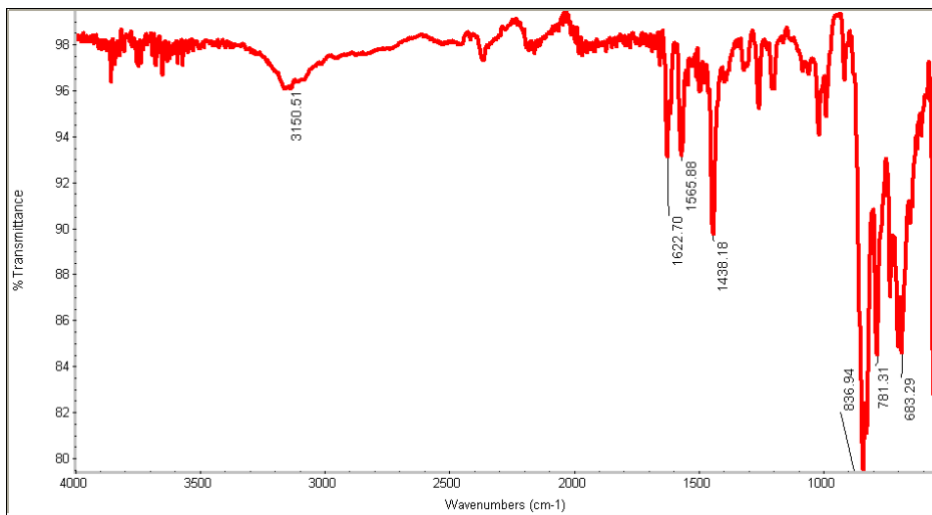


Figure A1.3. IR spectra of **3**

APPENDIX 2: MALDI SPECTRA

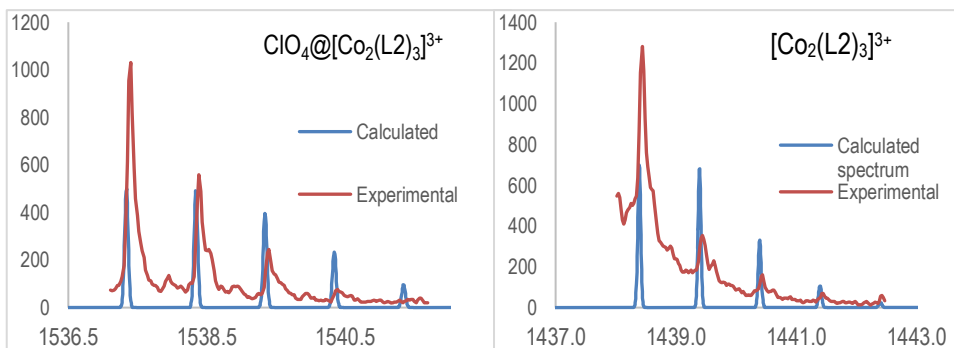


Figure A2.1. MALDI spectra for **1**. Match of calculated and experimental isotopic distribution of dinuclear helicate encapsulating ClO_4^- , $\text{ClO}_4@[\text{Co}_2(\text{L}2)_3]^{3+}$ (right), and dinuclear helicate $[\text{Co}_2(\text{L}2)_3]^{3+}$ (left).

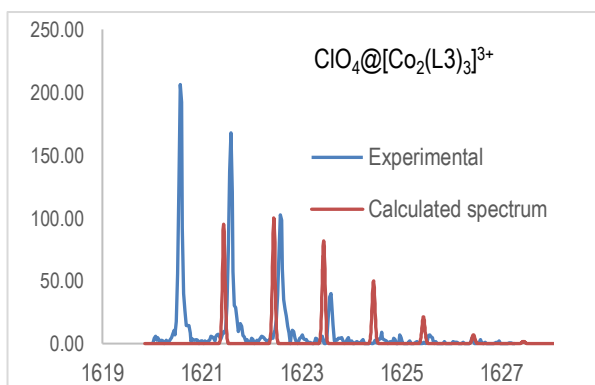


Figure A2.2. MALDI spectra for **2**. Match of calculated and experimental isotopic distribution of dinuclear helicate encapsulating ClO_4^- , $\text{ClO}_4@[\text{Co}_2(\text{L}3)_3]^{3+}$.

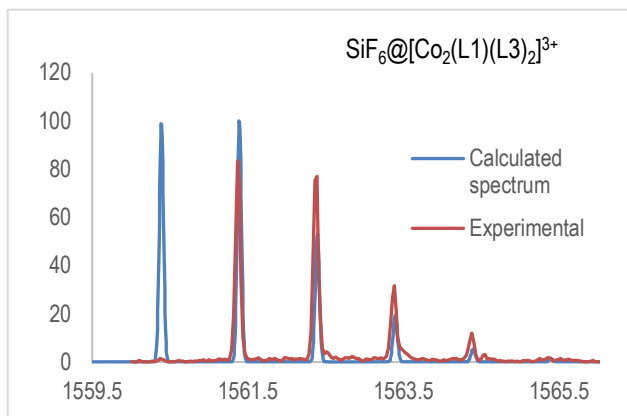


Figure A2.3. MALDI spectra for **3**. Match of calculated and experimental isotopic distribution of dinuclear helicate encapsulating SiF_6^{2-} , $\text{SiF}_6@[\text{Co}_2(\text{L}1)(\text{L}3)_2]^{3+}$.

